

## Al-BASED NANOQUASICRYSTALLINE ALLOYS WITH GOOD COLD WORKABILITY AND HIGH IMPACT FRACTURE ENERGY

Akihisa INOUE\*, Hisamichi KIMURA\*, Kenichiro SASAMORI\* and Kazuhiko KITA\*\*

\*Institute for Materials Research, Tohoku University, Sendai 980-8577, Japan

\*\*Graduate School, Tohoku University

**ABSTRACT** Melt-spun Al-Mn-TM and Al-Cr-TM (TM=Fe, Co, Ni or Cu) alloys in the ranges of 3 to 6 at%Mn (or Cr) and 1 to 4 at%TM consisted of nanoscale icosahedral (I) particles with a size of 30 to 50 nm surrounded by Al phase with a thickness of about 10 nm. The volume fraction of the I phase is 60 to 70 %. The similar mixed phase alloys in a bulk form were prepared by extrusion of their atomized powders. The bulk alloys exhibit good mechanical properties, i.e., high tensile strength of 500 to 800 MPa, large elongation up to 32 %, high fatigue strength of 240 MPa, cold workability by cold rolling, high Charpy energy reaching 180 kJ/m<sup>2</sup> and high elevated temperature strength of 250 MPa at 573 K. The new nanostructure and useful engineering properties are expected to enable practical uses of the nanostructure alloys as a new type of high functional Al-based alloys.

**Keywords:** nanoquasicrystalline alloy, powder metallurgy, mechanical strength, Charpy test, workability

## 1. INTRODUCTION

Although the quasicrystalline alloys reported up to date can be divided into the four kinds of icosahedral (I)[1], decagonal (D)[2], dodecagonal[3] and octagonal[3] phases, the quasicrystals which are composed of a single phase have been limited to the I and D phases[3]. It is known that the I-phase is formed in a number of Al-based alloys containing Mn, Cr, V, Fe, Cu or Pd as W elements[3]. The I-phase in the Al-M base systems has been reported to be composed of the Mackay I-clusters containing 55 atoms which are arranged through glue atoms to the three dimensional quasiperiodic lattice[4]. By the use of the large unit volume and a number of constituent atoms in the I-structure, it is highly expected that a subnanoscale control of the I-structure enables the improvement of ductility and toughness and the achievement of high magnetization. In this paper, we present the data of the achievement of high tensile strength and good ductility for the I base alloys in Al-based system.

## 2. DEFORMATION MECHANISM OF AN ICOSAHEDRAL PHASE ITSELF

In order to fabricate a new material with good mechanical properties, it is necessary to understand the deformation and fracture behavior of the I-phase itself. It is known[5] that the I-alloy can contain dislocations. However, the movement of the dislocations is difficult at elevated temperatures because the movement of the dislocations causes the destroy of the quasiperiodic lattice[7]. This fact indicates that the deformability of the I-alloy must be accomplished by the other mechanism. We have succeeded[6] in preparing a large single Al<sub>70</sub>Pd<sub>20</sub>Mn<sub>10</sub> I ingot by the Czochralski technique and the maximum size reaches 12 mm in diameter and 140 mm in length. In the nominal compressive stress-strain curves at various temperatures for the single quasicrystal[7], no plastic elongation is seen in the temperature range below 1000 K and the further increase in testing temperature causes a significant elongation. The flow stress at 1073 K is 650 MPa which is higher than that of a Ni<sub>3</sub>Al compound. The Young's modulus at room temperature is 200 GPa which is about 3 times higher than that for conventional Al-based alloys. The plastic deformation of the Al<sub>70</sub>Pd<sub>20</sub>Mn<sub>10</sub> single quasicrystal at temperatures above 1000 K takes place along the severely limited deformation bands. The Al concentration at the deformation bands increases and the deformation-induced deviation of alloy components has been detected. The deformation bands lie along the five-fold planes which are a closed packed plane. Besides, one can see the contrast of the precipitates with a pentagonal shape. The pentagonal precipitates have been confirmed[7] to have an approximant crystalline structure by the TEM analysis. From these experimental results, we have proposed[7,8] that the plastic deformation takes place through the following process; the generation of strain by application of load introduces linear phasons as well as the deviation of alloy components, leading to the

formation of approximant crystalline phases with periodic atomic configuration. It is therefore presumed that the plastic deformation takes place preferentially at the interface between I and approximant crystalline phases. Here, one can notice that the anomalous deformation mode comes from the unique transformation behavior. It is known[9] that the mismatch of tiling in the construction of penrose tiling pattern forms small regions with periodic atomic configuration by introduction of phason defects. By the deviation of two-dimensional quasiperiodic lattice points, we can obtain one dimensional approximant crystalline phases accompanying the formation of phason defects[9]. The transformation of the I phase to approximant crystalline phases can take place on a subnanoscale. By utilizing the anomalous deformation mode resulting from the unique transformation behavior, we can expect to fabricate a quasicrystal which is deformed at room temperature. The refinement to a nanoscale size and the deviation of alloy component to Al-rich range introduce a high density of phason defects into the nanoscale I phase, leading to the formation of coexistent I and approximant crystalline phases at Al-rich compositions.

### 3. RAPIDLY SOLIDIFIED STRUCTURE AND MECHANICAL PROPERTIES

The possibility of the above-described nanoscale structure control was examined for melt-spun Al-Mn-Ln[10,11] and Al-Cr-Ln[12,13] alloys. These alloy systems were chosen because Al-Mn[1] and Al-Cr[14] alloys are I-forming systems and Ln is the most effective element to increase the quenching effect for Al-TM alloys[15]. Figure 1 shows the compositional dependence of structure and mechanical properties of the melt-spun Al-Mn-Ce alloys[10]. It is to be noticed that the mixed fcc-Al and I phases are formed in the high Al concentration range above 92 at%Al and the mixed phase alloys exhibit good bend ductility and high  $\sigma_f$  reaching 1320 MPa. Figure 2 shows the bright-field electron micrograph and electron diffraction pattern of the melt-spun  $\text{Al}_{92}\text{Mn}_6\text{Ce}_2$  alloy with the highest  $\sigma_f$ . The structure consists of spherical I-particles with a size of 30 to 50 nm surrounded by a thin Al phase with a thickness of about 10 nm. It is to be noticed that the nanoscale I-particles disperse in an isolated state at the nanoscale interparticle spacing. The reflection rings come from the I-particles, indicating that these I-particles have random orientations because of the solidification mode of the primary precipitates of the I-phase, followed by the solidification of fcc-Al phase from the remaining liquid. Besides, one can see significant scattering of reflection rings, suggesting that the I-particles contain a high density of phason defects and approximant crystalline phase fields. Here, it is to be noticed that the volume fraction of the I-phase is as high as about 70 %.

A similar finely mixed structure has been obtained for Al-Cr base alloys[12,13]. As an example, Fig. 3 shows the bright- and dark-field images and the electron diffraction pattern of a melt-spun  $\text{Al}_{94.5}\text{Cr}_3\text{Ce}_1\text{Co}_{1.5}$  alloy with high  $\sigma_f$  of 1340 MPa. The dark-field image was taken from

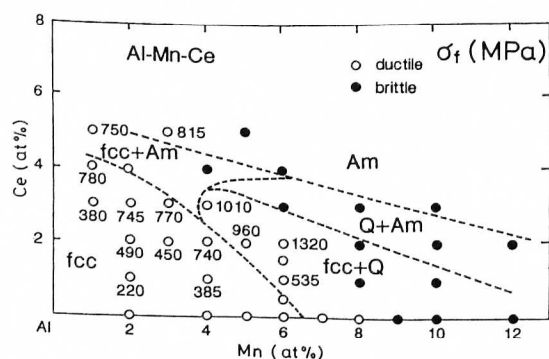


Fig. 1 Compositional dependence of tensile fracture strength ( $\sigma_f$ ) for rapidly solidified Al-Mn-Ce alloys.

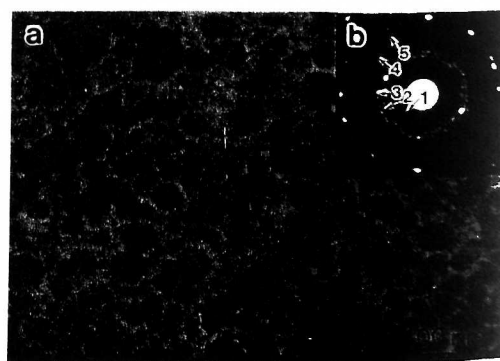


Fig. 2 Bright-field electron micrograph (a) and selected area diffraction pattern (b) of rapidly solidified  $\text{Al}_{92}\text{Mn}_6\text{Ce}_2$  alloy.

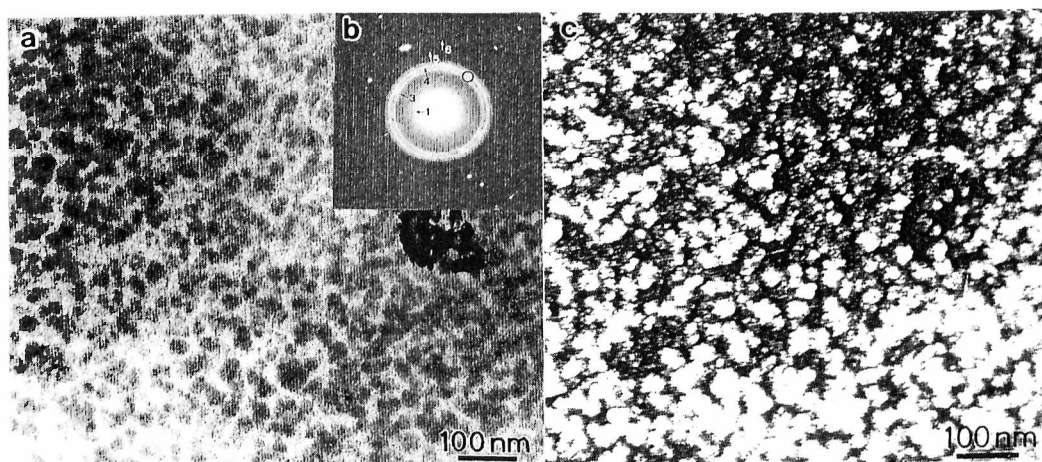


Fig. 3 Bright-field electron micrograph (a), selected area diffraction pattern (b) and dark-field electron micrograph (c) taken from a part of  $(211111)_i$  and  $(221001)_i$  reflection rings for a rapidly solidified  $\text{Al}_{94.5}\text{Cr}_3\text{Ce}_1\text{Co}_{1.5}$  alloy.

a part of  $(211111)_i$  and  $(221001)_i$  reflection rings. It is seen that I-particles with a size of 10 to 30 nm distribute homogeneously and the surrounding Al phase does not contain high-angle grain boundaries. The structural features are thought to result from the unique solidification mode which consists of the precipitation of the primary I-phase, followed by the solidification of the Al phase from the remaining liquid. The appearance of the reflection rings similar to halo rings suggests that the nanoscale particles have a highly disordered I-structure. The high  $\sigma_f$  exceeding 1000 MPa is also obtained for melt-spun  $\text{Al}_{93.5}\text{Cr}_3\text{Co}_{1.5}\text{Ce}_1\text{M}_1$  ( $\text{M}=\text{Ti}, \text{Mn}, \text{Fe}, \text{Co}, \text{Ni}, \text{Cu}, \text{Zr}$  or  $\text{Mo}$ ) alloys and the highest  $\sigma_f$  reaches 1350 MPa for  $\text{Al}_{93.5}\text{Cr}_3\text{Co}_{1.5}\text{Ce}_1\text{Ti}_1$ .

#### 4. INTERNAL STRUCTURE OF NANOSCALE ICOSAHERAL PHASE AND REASONS FOR HIGH TENSILE STRENGTH AND GOOD DUCTILITY

We examined the internal structure of the I-phase by the high-resolution TEM technique[13]. The HRTEM image shown in Fig. 4 was taken from the I-phase field in the melt-spun  $\text{Al}_{94.5}\text{Cr}_3\text{Ce}_1\text{Co}_{1.5}$  alloy. No contrast revealing the five-fold atomic configuration is seen over the whole image. One can see a modulated contrast typical for an amorphous phase over almost all the area, though there are small regions with fringe contrast corresponding to fcc-Al phase. The nanobeam electron diffraction pattern taken from the small region (B) with a diameter of 1 nm in the modulated contrast region consists only of halo rings. The structural features in which the modulated contrast is observed in the HRTEM image and the halo rings appear in the nanobeam diffraction pattern have been observed in the other I-phase fields. However, in the nanobeam diffraction pattern taken from the region with a diameter of 3 nm, the reflection spots with a five-fold

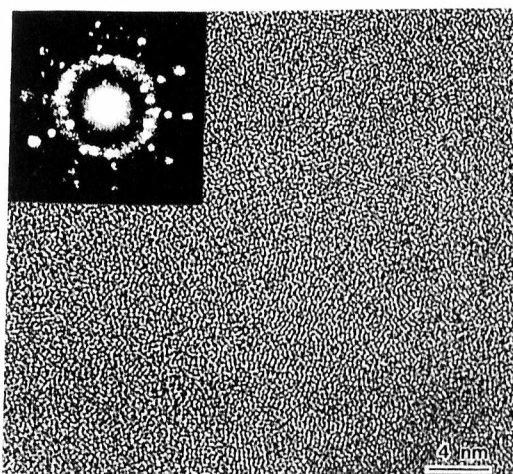


Fig. 4 High-resolution transmission electron micrograph and selected area electron diffraction pattern of rapidly solidified  $\text{Al}_{94.5}\text{Cr}_3\text{Ce}_1\text{Co}_{1.5}$  alloy.

symmetry have scarcely been observed in the superimposed state with halo rings. These data indicate that the I-particles with a size of 10 to 30 nm have a disordered atomic configuration on a short-range scale less than about 1 nm and an I atomic configuration on a long-range scale above about 3 nm. The short-range disorder and long-range I structure seems to be a new type of nonequilibrium structure which is different from amorphous, quasicrystalline and crystalline structures. The new nonequilibrium structure has the following features; (1) existence of attractive bonding nature between major (Al) and other minor atoms, (2) absence of slip planes, (3) existence of voids which enable the local movement of the constituent atoms, (4) unfixed atomic configurations leading to structural relaxation, and (5) existence of Al-Al bonding pairs because of the Al-rich concentrations. These features are nearly the same as those for metallic amorphous alloys with high  $\sigma_f$  and good ductility. It is therefore presumed that the similarity is the origin for the achievement of high  $\sigma_f$  and good ductility for the I base alloys.

##### 5. BULK ICOSAHEDRAL BASE ALLOYS PREPARED BY EXTRUSION OF ATOMIZED ICOSAHEDRAL POWDERS

We have confirmed[16] that the I base structure caused by rapid solidification can be kept up to annealing for 3.6 ks at 823 K. The high stability of the I base structure enables the production of bulk I base alloys by extrusion of atomized I base powders in the range of 573 to 673 K well below the decomposition temperature of the I phase. Figure 5 shows the correlation between  $\sigma_f$  and elongation for the bulk I base alloys in Al-Mn-Ce-Co and Al-Cr-Ce-Co systems, along with the data of commercial Al-based alloys and bulk nanogranular Al alloys obtained by extrusion of amorphous powders at temperatures above  $T_x$ . The bulk I base alloys exhibit high  $\sigma_f$  combined with large elongation which is 2 to 3 times larger than those for conventional high-strength Al alloys. The bulk I alloys also exhibit high elevated temperature strength above 200 MPa at 573 K which is 5 to 10 times higher than those for age-hardening Al alloys. Furthermore, the Young's modulus of the bulk I base alloys at room temperature is as high

as 97 to 102 GPa which are about 1.5 times higher than those for conventional Al alloys. It is thus summarized that the bulk I base alloys have the following features; (1) new nanostructure with short-range disorder and long-range quasiperiodicity, (2) new strengthening mechanism, (3) high specific strength, (4) high specific modulus, (5) high ductility leading to excellent formability, and (6) high elevated-temperature strength. These features allow us to expect that the present I base alloys develop as a new type of high-strength Al alloys.

We have subsequently found that a similar mixed structure consisting of nanogranular particles surrounded by fcc-Al phase without high-angle grain boundaries is also formed in melt-spun Al-Mn-M and Al-Cr-M (M=Fe, Co, Ni, Cu) alloys. The precipitation of the I phase increases the  $\sigma_f$  to the high values above 1000 MPa. The absence of Ln elements also increases  $\sigma_f$  for the extruded bulk alloys and the largest  $\epsilon_p$  reaches 30 % in the maintenance of  $\sigma_f$  of 500 MPa. In addition to the large  $\epsilon_p$ , the bulk I-based Al-Mn-M alloys exhibit a high impact fracture energy reaching 18 kJ/m<sup>2</sup> which is 1.5 times larger than that (12 kJ/m<sup>2</sup>) for the 7075-T6 alloy. We have also confirmed that the extruded bulk I base alloys are deformed up to about 70 % reduction in thickness (Re) even at room temperature.

##### 6. MECHANISM FOR HIGH DUCTILITY AND HIGH TOUGHNESS

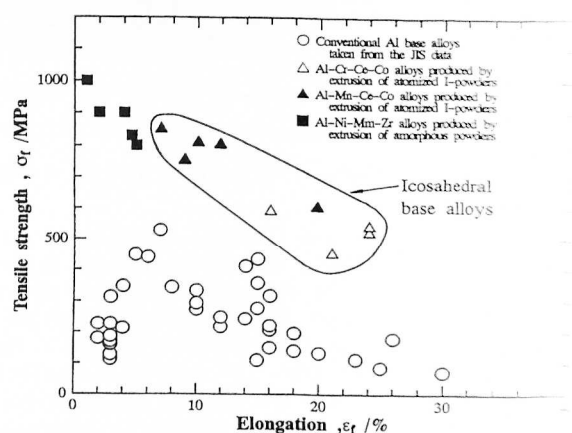


Fig. 5 Relation between tensile strength and elongation for bulk nanoquasicrystalline alloy in  $\text{Al}_{92}\text{Mn}_8\text{Ce}_2$  and  $\text{Al}_{94.5}\text{Cr}_3\text{Ce}_1\text{Co}_{1.5}$  systems produced by warm extrusion of atomized icosahedral base powders. JIS is the Japanese Institute of Steel.

In order to investigate the reason for the notable combination of high  $\sigma_f$ , large  $\varepsilon_p$ , high  $E_p$  and good cold deformability, we examined the effect of cold rolling on the microstructure and mechanical properties for the melt-spun Al-Cr-Ce-Co and Al-Mn-Ce alloys consisting mainly of nanogranular I phase[17]. These ribbon samples of 20  $\mu\text{m}$  in thickness can be cold rolled up to about 70 % Re in the absence of appreciable crack and tear failures. A number of deformation markings were observed over the whole surface region, but no crack was seen. The I base alloys have a good cold workability. Figure 6 shows the change in  $\sigma_f$  and  $H_v$  as a function of Re for the I base Al-Cr-Ce-Co and Al-Mn-Ce alloys. The  $\sigma_f$  and  $H_v$  decrease significantly by cold rolling, indicating a distinct work-softening phenomenon. This change is in contrast to the ordinary work-hardening phenomenon in which the  $\sigma_f$  and  $H_v$  increase for the cold-rolled samples. The distinct work-softening may be the reason for the achievements of large  $\varepsilon_p$ , high  $E_p$  and good cold-workability.

With the aim of clarifying the reason for the work softening for the I base alloys, we examined the microstructure of the cold-rolled samples. Figure 7 shows TEM images of the as-spun and 70% rolled  $\text{Al}_{92}\text{Mn}_6\text{Ce}_2$  amples[17]. The particle size of the I phase decreases from about 30 nm to about 10 nm by cold rolling to 50 %Re, accompanying a decrease in the interparticle spacing from 15 to 5 nm. The decreases in the particle size and interparticle spacing of the I-phase allow us to interpret that the I-phase itself was deformed plastically

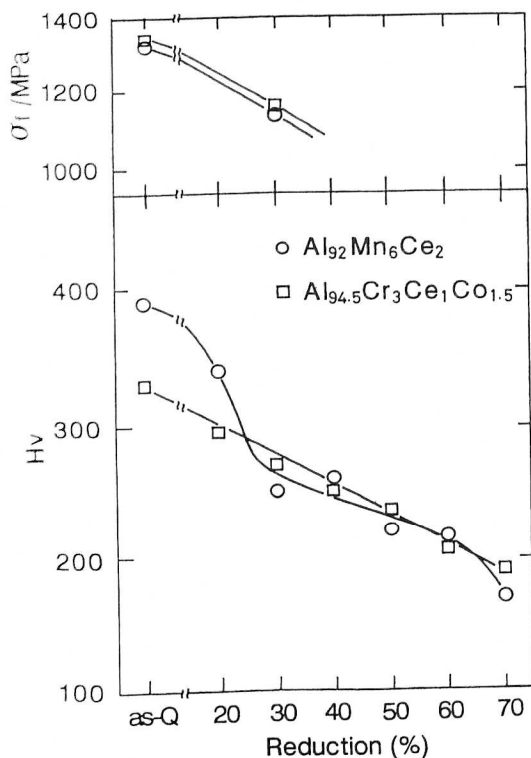


Fig. 6 Vickers hardness ( $H_v$ ) and tensile fracture strength ( $\sigma_f$ ) as a function of reduction in thickness (Re), for the melt-spun  $\text{Al}_{92}\text{Mn}_6\text{Ce}_2$  and  $\text{Al}_{94.5}\text{Cr}_3\text{Ce}_1\text{Co}_{1.5}$  ribbons subjected to cold rolling.

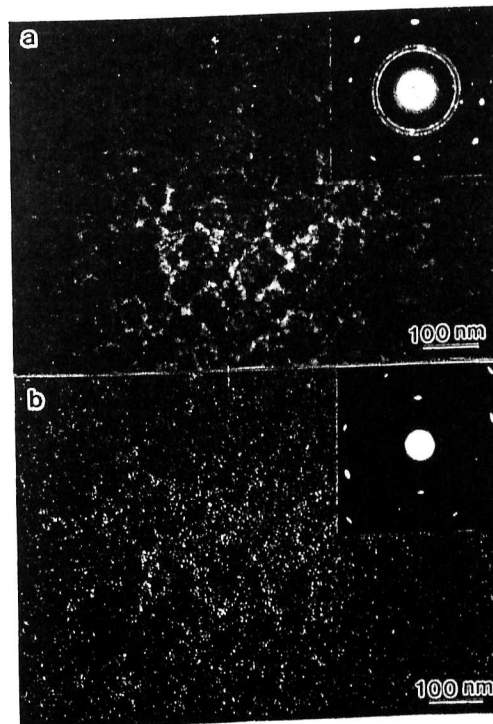


Fig. 7 Bright-field electron micrographs and selected-area electron diffraction patterns of  $\text{Al}_{92}\text{Mn}_6\text{Ce}_2$  ribbons in the as-spun (a) and 70% rolled (b) states.

and fragmented by slipping-off mechanism etc. because the plastic deformation of I-phase takes place in a narrow limited region. When the I-phase is fragmented, small voids seem to generate at the interface between I and Al phases. However, since the Al phase without grain boundary has high deformability, the voids are expected to be simultaneously embedded by the Al phase. Considering that no distinct dislocations are observed in the fcc-Al phase even for the cold-rolled samples, deformation-induced dislocations are sunk at the interface between I and Al phases. A similar structural change is observed for the  $\text{Al}_{92}\text{Mn}_6\text{Ce}_2$  alloy subjected to cold rolling to 50 and 70 % Re. In the 70 % Re sample, the structure is too fine to identify each I

particle. From these structural changes, it is thought that the work-softening phenomenon is due to the combination of (1) the increase in the volume fraction of the interface between I and Al phases caused by the refinement of I-particles by cold rolling and (2) the sinking of dislocations at the interface as is evidenced from the absence of appreciable dislocations in the cold-rolled I- and Al phases. The work-softening is also supported from the relation that the grain and/or particle sizes of the cold-rolled samples are located in the inverse Hall-Petch size region. The previous data[18] indicate that the inverse Hall-Petch phenomenon occurs in the grain size region less than about 30 nm. Figure 8 summarizes the mechanical properties of the newly developed I-phase bulk alloys in comparison with those[19] for the 7075-T6 alloy. All the properties except the coefficient of thermal expansion are superior to those for the 7075-T6 alloy and hence the I-base bulk alloys are expected to be used as a new type of high-strength structural material.

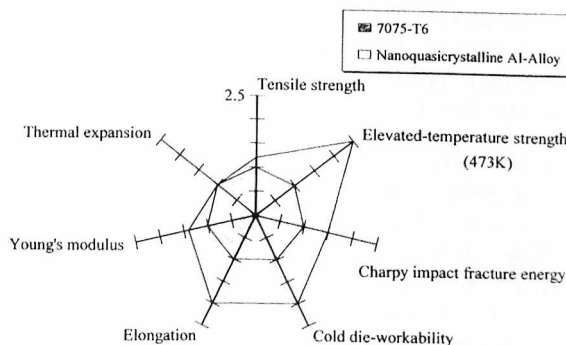


Fig. 8 Comparison of mechanical properties of nanoquasicrystalline Al-alloys with those of the 7075-T6 alloy.

## REFERENCES

1. D. Shechtman, I. Blech, D. Gratias and J.W. Cahn: Phys. Rev. Lett., 53(1984), 1951.
2. L. Bendersky: Phys. Rev. Lett., 55(1985), 1461.
3. S. Takeuchi: Quasicrystals, Sangyotosho, Tokyo, (1992).
4. A.L. Mackay: Sov. Phys. Crystallogr., 26(1981), 517.
5. S. Takeuchi: Tetsu-to-Hagane, 78(1987), 1517.
6. Y. Yokoyama, T. Miura, A.P. Tsai, A. Inoue and T. Masumoto: Mater. Trans., JIM, 33(1992), 97.
7. Y. Yokoyama, A. Inoue and T. Masumoto: Mater. Trans., JIM, 34(1993), 135.
8. A. Inoue, Y. Yokoyama and T. Masumoto: Mater. Sci. Eng., A181/A182(1994), 850.
9. Y. Ishii: Phys. Rev., B39(1989), 11862.
10. A. Inoue, M. Watanabe, H.M. Kimura, F. Takahashi, A. Nagata and T. Masumoto: Mater. Trans., JIM, 33(1992), 723.
11. M. Watanabe, A. Inoue, H.M. Kimura, T. Aiba and T. Masumoto: Mater. Trans., JIM, 34(1993), 162.
12. A. Inoue, H.M. Kimura, K. Sasamori and T. Masumoto: Mater. Trans., JIM, 35(1994), 85.
13. A. Inoue, H.M. Kimura, K. Sasamori and M. Watanabe: Mater. Trans., JIM, 36(1995), 6.
14. A. Inoue, H.M. Kimura and T. Masumoto: J. Mater. Sci., 22(1987), 1758.
15. A. Inoue, K. Ohtera and T. Masumoto: Jpn. J. Appl. Phys., 27(1988), L736.
16. A. Inoue, H.M. Kimura, K. Sasamori and K. Kita: New Horizons in Quasicrystals, ed. by A.I. Goldman et al., World Scientific, Singapore, (1997), p.256.
17. A. Inoue, H.M. Kimura, M. Watanabe and A. Kawabata: Mater. Trans., JIM, 38(1997), 756.
18. K.A. Padmanabhan and H. Hahn: Synthesis and Processing of Nanocrystalline Powder, ed. by D.L. Bourell, TMS, Warrendale (1996), p.21.
19. J.T. Staley: Aluminum Alloys, ed. by A.K. Vasudevan and R.D. Doherty, Academic Press Inc., San Diego, (1989), p.17.